Modularized Control Strategy and Performance Analysis of DFIG System Under Unbalanced and Harmonic Grid Voltage

Yipeng Song, *Student Member, IEEE*, and Heng Nian, *Member, IEEE*

***Abstract*—The paper presents a modularized control strategy of doubly fed induction generator (DFIG) system, including the grid-side converter (GSC) and rotor-side converter (RSC), under unbalanced and harmonic grid voltage. The sequence decomposition process and complicated control reference calculation can be avoided in the proposed control strategy. From the perspective of power grid friendly operation, the control targets of DFIG system in this paper are chosen as: 1) smooth active and reactive power injected into the power grid; 2) balanced and sinusoidal current injected into the power grid. The RSC and GSC can work as two independent modules and the communication between RSC and GSC can be removed. Furthermore, the third harmonic current component, dc-link voltage fluctuation, and electromagnetic torque pulsation under the different control targets are theoretically analyzed. Finally, the availability of the proposed modularized control strategy of DFIG system under unbalanced and distorted grid voltage is verified by experiment results.**

***Index Terms*—Balanced and sinusoidal current, doubly fed induction generator (DFIG) system, modularized control, smooth active and reactive power, unbalanced and harmonic grid voltage.**

I. Introduction

WIND power generation based on the doubly fed induction generator (DFIG) has gained increasing popularity due to its advantages of smaller converters rating around 30% of the generator rating, variable speed, and four-quadrant active and reactive power operation capabilities. Several control strategies have been investigated to improve the power generation performance of DFIG under the ideal grid voltage, i.e., the vector oriented control (VOC) [1], direct power control (DPC) [2], etc. However, the grid voltage may always contain negative and harmonic component in practical situation [3], [4], and the DFIG system operation performance would be jeopardized if the unbalanced and distorted components in the grid voltage are not taken into consideration.

Up to now, several effective control strategies of the rotor-side converter (RSC) and the grid-side converter (GSC) in DFIG system under grid voltage unbalance, or harmonically distortion, or unbalanced and harmonic distortion condition, have been investigated based on VOC [5]–[11] and DPC [12]–[16]. The several control targets were selected to improve the DFIG operation performance under the nonideal grid conditions, for instance, balanced stator output current, smooth stator output active/reactive power, smooth electromagnetic torque, etc. In [5], [8], [9], and [12] the coordinated control of both GSC and RSC under the nonideal grid voltage conditions has been proposed. Generally, in the coordinated control, RSC was controlled to obtain the smooth DFIG electromagnetic torque and GSC was controlled to ensure the overall smooth active power injected by both the RSC and GSC into the power grid [5], [8], [12]. While Yao *et al*. [9] employed the series GSC (SGSC) to the conventional DFIG system topology, the nonideal grid voltage condition can be well compensated by the SGSC and the DFIG can operate under normal grid voltage condition all the time.

However, the previous works also contain certain drawbacks that would be unbeneficial for the practical applications:

1) In order to achieve the specific control targets under the nonideal grid condition, the fundamental, negative, and harmonic components of grid voltage have to be extracted [5]–[13]. The extraction procedure would employ many notch filters and low-pass filters; as a result, the phase delay and control error would be inevitable.
2) In order to implement the different control targets by employing VOC [5]–[11] or DPC [12]–[13] strategy, the control reference calculation of rotor current in VOC or active/reactive power in DPC is always complicated and time consuming. Furthermore, DFIG parameters deviation, as well as the fundamental, negative, and harmonic component change of grid voltage would also deteriorate the reference calculation accuracy and control target implementation.
3) In order to achieve the smooth active power output of DFIG system to the grid, the conventional control strategy, similar as [5], would allow the existence of active power pulsation in the RSC, while the GSC is controlled to generate the opposite active power pulsation of same quantity as RSC, so as to maintain the overall smooth active power output of DFIG system. However, in order to realize that the GSC needs to communicate all the time with the RSC to acquire the accurate information of active power pulsation in the RSC, this would inevitably increase the DFIG system complexity and reduce the operation reliability.

Liu *et al*. [17] proposed the stator harmonic current elimination technique by applying the closed-loop resonant controller for the stator current in RSC control. Since the stator harmonic

Manuscript received April 24, 2014; revised August 21, 2014; accepted October 28, 2014. Date of publication October 31, 2014; date of current version April 15, 2015. Recommended for publication by Associate Editor M. Malinowski.

The authors are with the College of Electrical Engineering, Zhejiang University, Hangzhou 310027, China (e-mail: eedqgcsyp@126.com; nianheng@zju.edu.cn).

Color versions of one or more of the figures in this paper are available online at http://ieeexplore.ieee.org.

Digital Object Identifier 10.1109/TPEL.2014.2366494

current is directly regulated by the resonant controller, the complicated rotor current reference calculation and harmonic components extraction can be avoided. However, the control target of RSC is single and only the sinusoidal stator current can be implemented, while the voltage unbalance and GSC control are neglected.

This paper proposes the modularized control strategy of DFIG system under unbalanced and distorted grid voltage to avoid the communication between RSC and GSC, and the grid voltage fundamental, negative, and harmonic components extraction, as well as complicated reference calculation, can also be avoided. From the perspective of power grid friendly operation of DFIG system, the control targets of DFIG system are chosen as: 1) smooth active and reactive power of RSC and GSC into the power grid; 2) balanced and sinusoidal current of RSC and GSC injected into the power grid. Indeed, the DFIG electromagnetic torque ripple deserves much attention for the purpose of safe and reliable operation of mechanic components. However, it has been reported in [10] that the achieving of balanced and sinusoidal stator current would inevitably cause the electromagnetic torque ripple of 100 and 300 Hz, which means these two control targets are contradictory. In this paper, the authors tend to focus more on the wind power quality, rather than the reliable operation of mechanic components; therefore, the control targets of this paper are chosen as, balanced and sinusoidal stator current, or the smooth active and reactive power. The control target of eliminating the DFIG electromagnetic torque ripple can be investigated in the future work.

This paper is organized as follows: in Section II, the mathematical model of a DFIG system under negative, fifth, and seventh harmonically distorted grids is briefly mentioned. The proposed modularized control strategy is described in detail in Section III. The occurrence of third harmonic current component under control Target I, the dc-link voltage fluctuation, and electromagnetic torque pulsation under both control targets are also theoretically analyzed in Section IV. The VPI regulator's robustness against DFIG parameters deviation is also analyzed in Section IV. Finally, in Section V, the experimental system on 1 kW laboratory DFIG system is developed to validate the availability of the modularized control strategy of DFIG system.

II. Mathematical Model of DFIG RSC and GSC Under Unbalanced and Distorted Grid Voltage

Since the fifth and the seventh harmonic components are the major harmonic components in grid voltage [14], only these two harmonic components are taken into consideration in this paper. The mathematical model of DFIG system under unbalanced and harmonic grid voltage has been well established in [5] and is described briefly as follows.

The stator current can be presented as [5]

$$\boldsymbol{I}^{+}_{sdq} = \boldsymbol{I}^{+}_{sdq+} + \boldsymbol{I}^{-}_{sdq-}e^{-j2\theta_1} + \boldsymbol{I}^{5-}_{sdq5-}e^{-j6\theta_1} + \boldsymbol{I}^{7+}_{sdq7+}e^{j6\theta_1} \tag{1}$$

where **I** is the current; subscripts *d, q* represent components at the *d, q* axis; subscript *s* represents stator components of DFIG; superscripts $+$, $-$, $5-$, and $7+$ represent the $(dq)^{+}$, $(dq)^{-}$, $(dq)^{5-}$, and $(dq)^{7+}$ reference frames rotating at the angular speed of $+\omega_1$, $-\omega_1$, $-5\omega_1$, and $+7\omega_1$; subscripts $+$, $-$, $5-$, and $7+$ represent the fundamental, negative, fifth, and seventh harmonic components; θ_1 represents the phase angle of grid voltage fundamental component; and ω_1 represents the angular speed of grid voltage fundamental component.

Similarly, the grid voltage can be presented as

$$\boldsymbol{U}^{+}_{sdq} = \boldsymbol{U}^{+}_{sdq+} + \boldsymbol{U}^{-}_{sdq-}e^{-j2\theta_1} + \boldsymbol{U}^{5-}_{sdq5-}e^{-j6\theta_1} + \boldsymbol{U}^{7+}_{sdq7+}e^{j6\theta_1} \tag{2}$$

where **U** is the voltage.

Then, based on (1) and (2), the stator output active and reactive power of DFIG can be presented as [5]

$$\begin{aligned} P_s + jQ_s = & -\frac{3}{2}\Big(\boldsymbol{U}^{+}_{sdq+} + \boldsymbol{U}^{-}_{sdq-}e^{-j2\theta_1} + \boldsymbol{U}^{5-}_{sdq5-}e^{-j6\theta_1} \\ & + \boldsymbol{U}^{7+}_{sdq7+}e^{j6\theta_1}\Big) \\ & *\Big(\boldsymbol{I}^{+}_{sdq+} + \boldsymbol{I}^{-}_{sdq-}e^{j2\theta_1} + \boldsymbol{I}^{5-}_{sdq5-}e^{j6\theta_1} \\ & + \boldsymbol{I}^{7+}_{sdq7+}e^{-j6\theta_1} + \boldsymbol{I}^{3+}_{sdq3+}e^{j-2\theta_1}\Big) \end{aligned} \tag{3}$$

where $\hat{\boldsymbol{I}}^{+}_{sdq}$ is the conjugated vector of $\hat{\boldsymbol{I}}^{+}_{sdq}$, P_s and Q_s are the stator active and reactive power. When the control target of smooth active and reactive power is selected, the third harmonic component would exist in stator current, while the stator current negative component would be zero, the detailed explanation can be found in Section IV-A.

It can be found out from (3) that the active and reactive power under unbalanced and distorted grid voltage would contain dc average component, 100 and 300 Hz pulsation components, which are produced by the interaction between fundamental and negative harmonic components. Furthermore, the 200 and 400 Hz power pulsation components can also be produced by the interaction between negative and harmonic components; they can be neglected in the control strategy due to the tiny amplitude.

The mathematic model of GSC current, active and reactive power can be similarly expressed as

$$\begin{aligned} \boldsymbol{I}^{+}_{gdq} = & \ \boldsymbol{I}^{+}_{gdq+} + \boldsymbol{I}^{-}_{gdq-}e^{-j2\theta_1} + \boldsymbol{I}^{5-}_{gdq5-}e^{-j6\theta_1} \\ & + \boldsymbol{I}^{7+}_{gdq7+}e^{j6\theta_1} \end{aligned} \tag{4}$$

$$\begin{aligned} P_g + jQ_g = & -\frac{3}{2}\Big(\boldsymbol{U}^{+}_{gdq+} + \boldsymbol{U}^{-}_{gdq-}e^{-j2\theta_1} + \boldsymbol{U}^{5-}_{gdq5-}e^{-j6\theta_1} \\ & + \boldsymbol{U}^{7+}_{gdq7+}e^{j6\theta_1}\Big) \\ & *\Big(\boldsymbol{I}^{+}_{gdq+} + \boldsymbol{I}^{-}_{gdq-}e^{j2\theta_1} + \boldsymbol{I}^{5-}_{gdq5-}e^{j6\theta_1} \\ & + \boldsymbol{I}^{7+}_{gdq7+}e^{-j6\theta_1} + \boldsymbol{I}^{3+}_{gdq3+}e^{-j2\theta_1}\Big) \end{aligned} \tag{5}$$

where the subscript *g* represents the GSC component.

It should be noted that the $\boldsymbol{U}^{+}_{sdq}$ in (3) and $\boldsymbol{U}^{+}_{gdq}$ in (5) identically represent the grid voltage. When the control target of smooth active and reactive power is achieved, the third harmonic component would exist in the grid current, while the grid current negative component would be zero; the detail explanation can be found in Section IV-A.

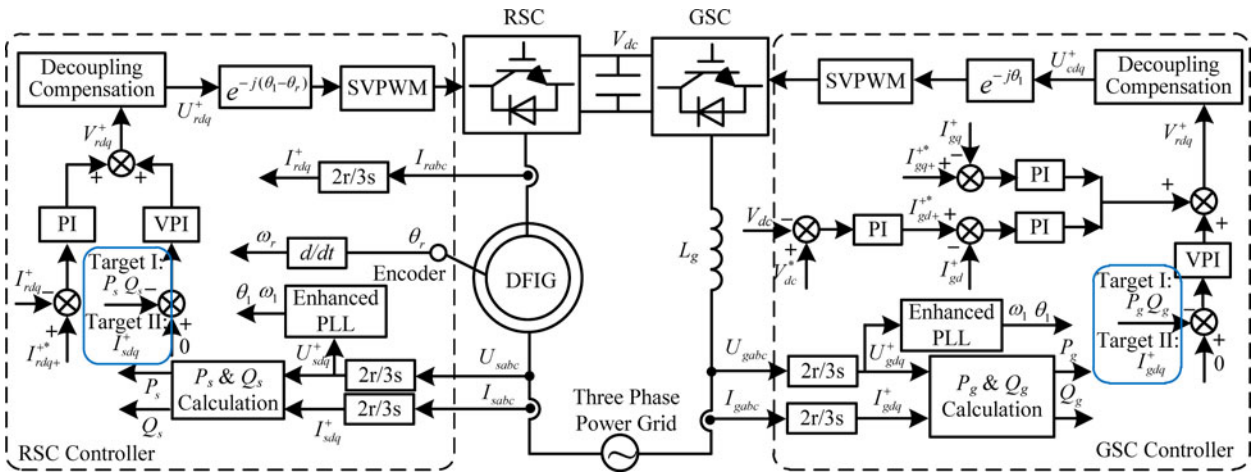

Fig. 1. Block diagram of the proposed modularized control strategy of DFIG system.

Therefore, based on the aforementioned discussion, it can be found out that when DFIG system works on the unbalanced and distorted grid, the unbalanced and harmonic current, as well as output active and reactive power pulsation, will be injected into the power grid, which is detrimental for the wind energy quality and unfavorable for the stable and reliable operation of power grid. It is of great importance to improve the injected wind energy quality in terms of either balanced and sinusoidal three-phase current or smooth active and reactive power outputted from DFIG system.

III. Proposed Modularized Control Strategy

A. Detailed Description

The modularized control strategy and block diagram for RSC and GSC is shown in Fig. 1. As shown in Fig. 1, RSC and GSC can work independently as two separate modules without the need for communication. The overall control targets for DFIG system can be defined as:

1) ***Target I:*** Smooth active and reactive power injected into the power grid.
2) ***Target II***: Balanced and sinusoidal current injected into the power grid.

1) RSC Control Strategy: In the RSC control strategy, the stator active and reactive power P_s and Q_s of DFIG can be calculated according to the stator voltage $\boldsymbol{U}^+_{sdq}$ and stator current $\boldsymbol{I}^+_{sdq}$ as shown in (3). The grid voltage phase angle θ_1 can be obtained by the PLL module based on the resonant regulator tuned at 100 and 300 Hz [12]. The rotor position θ_r can be obtained from the encoder. The closed-loop control of rotor current $\boldsymbol{I}^+_{rdq}$ can be implemented based on PI regulator to control the DFIG average output power, and the rotor current reference $\boldsymbol{I}^{+*}_{rdq+}$ can be obtained according to the power reference from the maximum power point track (MPPT) [11].

When the alternative control targets, i.e., smooth active and reactive power output or balanced and sinusoidal stator current, are chosen, the closed-loop control with vector proportional integral (VPI) regulator tuned at 100 and 300 Hz would be employed to directly regulate the negative and harmonic components of stator current, or the 100 and 300 Hz pulsation of stator output active and reactive power.

The output of PI regulator and VPI regulator that are added together with the decoupling compensation item [5] would finally achieve the rotor control voltage reference $\boldsymbol{U}^{+*}_{rdq}$, which would be used as the space vector pulse width modulation (SVPWM) module input to generate the IGBT switch signal for RSC.

2) GSC Control Strategy: In the GSC control strategy, the active and reactive power P_g and Q_g can be calculated according to the grid voltage $\boldsymbol{U}^+_{gdq}$ and current $\boldsymbol{I}^+_{gdq}$. The grid voltage phase angle θ_1 can be obtained by the PLL module based on the resonant regulator tuned at 100 and 300 Hz [12]. Since the major function of GSC is to provide stable dc-link voltage $V_{\rm dc}$ [5], [8], [12], the closed-loop control of dc-link voltage is implemented based on PI regulator, and the output is considered as the d-axis current reference $\boldsymbol{I}^{+*}_{gd+}$. The $\boldsymbol{I}^{+*}_{gd+}$ and the q-axis current reference $\boldsymbol{I}^{+*}_{gd+}$ (which is normally set 0 to achieve unity power factor operation) would be used as the PI regulator input of current control loop to regulate the fundamental component of grid current.

When the alternative control targets, i.e., smooth GSC active and reactive power output or balanced and sinusoidal GSC current, are chosen, the closed-loop control with VPI regulator tuned at 100 and 300 Hz would be employed to directly regulate the GSC current negative and harmonic components, or the 100 and 300 Hz pulsation of GSC output active and reactive power. Then, the switch signal implementation process for GSC is the same as the control of RSC.

B. Advantage of Modularized Control Strategy

Based on the earlier description and control block diagram shown in Fig. 1, it can be found out that, when the DFIG system operates under the unbalanced and harmonic voltage, the advantages of the modularized control strategy over the conventional coordinated control strategy [5], [8], [12] can be concluded as follows:

1) In order to achieve the two alternative control targets, both RSC and GSC are able to operate independently and no communication is required; thus, the DFIG system control complexity can be simplified.
2) The negative and harmonic components extraction of grid voltage, stator current for RSC, or grid current for GSC can be avoided, and the complicated control reference calculation is also avoided. Thus, the RSC and GSC control complexity can be reduced.
3) The control reference calculation for both RSC and GSC with control Targets I and II is no longer needed in the proposed control strategy, then the DFIG system parameters is not involved in the control reference calculation; thus, the possibility of DFIG system parameters deviation to influence the control accuracy can be eliminated.

C. Limitation of Modularized Control Strategy

However, there are also limitations of the proposed modularized control strategy:

1) when the control Targets I and II are achieved, the electromagnetic torque 100 and 300 Hz pulsation would be produced, and the DFIG bearing and gear-box would be damaged as a consequence;
2) the dc-link voltage 100 and 300 Hz fluctuations would be generated when the control Targets I and II are implemented; therefore, for the safe operation of RSC and GSC, the dc-link capacitor needs to be increased;
3) the third harmonic component of stator current and GSC current would be produced when the control Target I is achieved; this is explained in detail in Section IV-A. Therefore, the current injected into the power grid may be further polluted.

D. VPI Regulator

For the purpose of achieving the alternative control targets with the proposed modularized control strategy, it is important to implement the accurate control of 100 and 300 Hz components. The VPI regulator [18]–[20], based on pole–zero cancellation to avoid the unexpected gain peak, can be used to eliminate the DFIG stator current or active and reactive power 100 and 300 Hz components control error (GSC three-phase current or active and reactive power 100 and 300 Hz) due to the adequate closed-loop phase margin and accurate ac signal tracking capability [14], [18]–[20]

$$C_{VPI} = \frac{K_{pr2}s^2 + K_{ir2}s}{s^2 + \omega_{c2}s + (2\omega_1)^2} + \frac{K_{pr6}s^2 + K_{ir6}s}{s^2 + \omega_{c6}s + (6\omega_1)^2} \quad (6)$$

where ω_{c2} and ω_{c6} are the resonant bandwidth of 100 and 300 Hz components to widen the resonant frequency and improve the VPI regulator robustness against grid frequency variation; ω_1 is the angular speed of grid voltage fundamental component; K_{pr2} and K_{ir2}, K_{pr6} and K_{ir6} are the proportional and integral coefficients of VPI 100 and 300 Hz components, respectively, and $K_{ir2} = K_{pr2}R_r/\sigma L_r$, $K_{ir6} = K_{pr6}R_r/\sigma L_r$ should be followed based on the rule of pole–zero cancellation for RSC control, and $K_{ir2} = K_{pr2}R_g/L_g$, $K_{ir6} = K_{pr6}R_g/L_g$ for GSC control [19], [20].

IV. Performance Analysis on Modularized Control Strategy

The two control targets can enhance the power quality outputted by the overall DFIG system. However, there is still some detrimental influence on the operation reliability of DFIG system. The following focuses on the performance analysis of DFIG system with the proposed modularized control strategy.

A. Analysis on Third Harmonic Current Under Target I

It was mentioned in [13] that, when the stator active and reactive power 100 Hz pulsation of DFIG are simultaneously removed, the third harmonic component in stator current would be generated as a consequence. However, only the qualitative analysis on the third harmonic current component was reported. Considering that the third harmonic current component would further pollute the power grid, it is essentially necessary to quantitatively investigate the third harmonic current component when the control Target I is achieved from the perspective of the safe and reliable operation of power grid.

It needs to point out that the third harmonic current component is produced to eliminate the active and reactive power 100 Hz pulsation caused by the grid voltage unbalance and is irrelevant to the grid voltage harmonic distorted components; therefore, the following discussion on the third harmonic current component would involve the negative sequence component of grid voltage only.

In the RSC control, the 100 Hz active and reactive power pulsations are mainly caused by the interaction between grid voltage negative component $\boldsymbol{U}^-_{sdq-}$ and the stator current fundamental component $\boldsymbol{I}^+_{sdq+}$, as well as the interaction between grid voltage fundamental component $\boldsymbol{U}^+_{sdq+}$ and the stator current negative component $\boldsymbol{I}^-_{sdq-}$ and third harmonic components [13]. It should be pointed out that, since VPI regulator tuned at 100 Hz in synchronous frame would generate the ± 100 Hz ac signals output due to VPI regulation capability for both $+100$ and -100 Hz ac error signal, the VPI regulator output would behave as -50 and $+150$ Hz ac signals in the stationary frame, which would finally result in the negative and third harmonic components in DFIG stator current, respectively. Importantly, the third harmonic component of DFIG stator current or the GSC three-phase current for eliminating fluctuations in active/reactive power output is different from the commonly known one (which is zero sequence with the three-phase current having the same phase angle); it is the positive sequence of 150 Hz. Thus, the three phases of the third harmonic current would have the phase angle of 300 $\pi t + 0°$ for Phase A, 300 πt$-120°$ for Phase B, and 300 πt$-240°$ for Phase C. As a result, the third harmonic component of DFIG stator current or the GSC three-phase current is able to flow.

According to (3), 100 Hz pulsation component of stator active and reactive power can be expressed as

$$\begin{aligned} P_{s100}+jQ_{s100} &= -\frac{3}{2}\Big(\boldsymbol{U}^{-}_{sdq-}\boldsymbol{I}^{+}_{sdq+}e^{-j2\theta_1} \\ &\quad +\boldsymbol{U}^{+}_{sdq+}\boldsymbol{I}^{-}_{sdq-}e^{j2\theta_1}+\boldsymbol{U}^{+}_{sdq+}\boldsymbol{I}^{3+}_{sdq3+}e^{-j2\theta_1}\Big) \\ &= -\frac{3}{2}\begin{pmatrix}(k_1+k_3+k_5)\cos 2\theta_1+(k_2-k_4+k_6)\sin 2\theta_1 \\ +j\,(k_2+k_4+k_6)\cos 2\theta_1+j\,(k_3-k_1-k_5)\sin 2\theta_1\end{pmatrix} \end{aligned} \tag{7a}$$

where

$$\begin{aligned} P_{s100\_\cos} &= -\frac{3}{2}(k_1+k_3+k_5) \\ P_{s100\_\sin} &= -\frac{3}{2}(k_2-k_4+k_6) \\ Q_{s100\_\cos} &= -\frac{3}{2}(k_2+k_4+k_6) \\ Q_{s100\_\sin} &= -\frac{3}{2}(k_3-k_1-k_5) \end{aligned} \tag{7b}$$

where

$$\begin{aligned} k_1 &= U^{-}_{sd-}I^{+}_{sd+}+U^{-}_{sq-}I^{+}_{sq+} \\ k_2 &= U^{-}_{sq-}I^{+}_{sd+}-U^{-}_{sd-}I^{+}_{sq+} \\ k_3 &= U^{+}_{sd+}I^{-}_{sd-}+U^{+}_{sq+}I^{-}_{sq-} \\ k_4 &= U^{+}_{sq+}I^{-}_{sd-}-U^{+}_{sd+}I^{-}_{sq-} \\ k_5 &= U^{+}_{sd+}I^{3+}_{sd3+}+U^{+}_{sq+}I^{3+}_{sq3+} \\ k_6 &= U^{+}_{sq+}I^{3+}_{sd3+}-U^{+}_{sd+}I^{3+}_{sq3+}. \end{aligned} \tag{7c}$$

Thus, based on (7b) and (7c), it can be seen that, in order to achieve smooth stator output active and reactive power, these equations need to be satisfied, $k_3=k_4=0$ $k_1+k_5=0$, and $k_2+k_6=0$. Thus, the following conclusion can be obtained:

1) According to $k_3=k_4=0$, it can be deduced that the negative component of stator current is null, i.e., $\boldsymbol{I}^{-}_{sdq-}=0$, which means no stator current negative components would be injected into the power grid under the control strategy I of smooth active and reactive power.
2) According to $k_1+k_5=0$, it can be found out that the d-axis component $I^{\boldsymbol{3+}}_{sd3+}$ of the third harmonic current is only related to the unbalanced voltage components and fundamental components of stator current (U^{+}_{sq+} should be 0 since d^{+} is aligned with the fundamental component of grid voltage)

$$I^{3+}_{sd3+}=-\frac{U^{-}_{sd-}I^{+}_{sd+}+U^{-}_{sq-}I^{+}_{sq+}}{U^{+}_{sd+}}. \tag{8a}$$

Similarly, according to $k_2+k_6=0$, the q-axis component of third harmonic current can be presented as

$$I^{3+}_{sq3+}=\frac{U^{-}_{sq-}I^{+}_{sd+}-U^{-}_{sd-}I^{+}_{sq+}}{U^{+}_{sd+}}. \tag{8b}$$

Based on (8a) and (8b), it can be concluded that, when the control target of smooth active and reactive power is achieved, the stator current third harmonic component would be produced and is relevant to the negative voltage component and the fundamental current component. The grid may be further polluted due to the injection of the third harmonic current into the power grid.

The third harmonic component $\boldsymbol{I}^{\boldsymbol{3+}}_{gdq3+}$ of GSC current can be deduced similarly and expressed as

$$\begin{aligned} I^{3+}_{gd3+} &= -\frac{U^{-}_{sd-}I^{+}_{gd+}+U^{-}_{sq-}I^{+}_{gq+}}{U^{+}_{sd+}} \\ I^{3+}_{gq3+} &= \frac{U^{-}_{sq-}I^{+}_{gd+}-U^{-}_{sd-}I^{+}_{gq+}}{U^{+}_{sd+}}. \end{aligned} \tag{9}$$

Therefore, based on (8a) and (8b) and (9), the overall third harmonic current components outputted from DFIG system can be presented as

$$\begin{aligned} I^{3+}_{alld3+} &= I^{3+}_{sd3+}+I^{3+}_{gd3+} \qquad (10a) \\ &= \frac{-\left(U^{-}_{sd-}\left(I^{+}_{sd+}+I^{+}_{gd+}\right)+U^{-}_{sq-}\left(I^{+}_{sq+}+I^{+}_{gq+}\right)\right)}{U^{+}_{sd+}} \\ I^{3+}_{allq3+} &= I^{3+}_{sq3+}+I^{3+}_{gq3+} \\ &= \frac{U^{-}_{sq-}\left(I^{+}_{sd+}+I^{+}_{gd+}\right)-U^{-}_{sd-}\left(I^{+}_{sq+}+I^{+}_{gq+}\right)}{U^{+}_{sd+}}. \end{aligned} \tag{10b}$$

It can be seen that, the overall third harmonic current component of DFIG system is determined by the unbalanced component of grid voltage U^{-}_{sdq-}, the fundamental component of grid voltage U^{+}_{sdq+}, the fundamental component of DFIG stator current I^{+}_{sdq+}, and the fundamental component of GSC current I^{+}_{gdq+}. As the grid voltage unbalance condition becomes severe, the third harmonic current would also be aggravated. Similarly, the increasing of DFIG system active and reactive power would also enhance the third harmonic current.

B. DC-Link Voltage Fluctuation Under Target I and Target II

In the DFIG system, the dc-link voltage is first established by the GSC and then is regarded as the stable dc power supply for the RSC to implement the safe and reliable operation of DFIG system. Under the control Targets I and II, 100 and 300 Hz fluctuation of dc-link voltage would occur inevitably. The dc-link voltage fluctuation will deteriorate the lifetime of dc-link capacitor, and the overlarge dc-link voltage fluctuation would cause the danger of IGBT overvoltage and even damage the entire hardware equipment. Therefore, from the perspective of the safe and reliable operation of DFIG system, it would be essentially meaningful to analyze the dc-link voltage fluctuation under unbalanced and distorted grid voltage condition with the control Targets I and II.

According to [5], the dc-link voltage would be influenced by the DFIG electromagnetic power, DFIG stator active power, and

GSC active power

$$C\frac{dV_{dc}}{dt}V_{dc} = P_e + P_s + P_g \tag{11}$$

where $V_{\rm dc}$ represents the dc-link voltage, C is dc-link capacitor, P_e, P_s, and P_g are the electromagnetic power, DFIG stator active power, and GSC active power, respectively.

It should also be noted that the instantaneous active power pulsation in the GSC inductance L_g is not null, but due to its significant small value compared with the P_e, P_s, and P_g in (11), the following discussion would ignore the instantaneous active power pulsation in the GSC inductance L_g.

The power positive direction in this discussion is defined as flowing from power grid to the DFIG system; therefore, in (11), P_e is always positive due to the electromagnetic power from wind turbine to the DFIG, P_s is always negative due to the generator characteristic of DFIG, and P_g is positive under subsynchronous state, or negative under supersynchronous state.

Based on (11), it can be seen that the dc-link voltage is determined by the three active power components, thus these active power pulsation needs to be investigated first.

1) Active Power Pulsation Under Control Target I: As described in Section IV-A, when control Target I is achieved, no stator and grid current negative components would be produced. Therefore, the 100 Hz electromagnetic power pulsation can be presented as [17]

$$P_{e2}^I = \frac{3}{2}\omega_r \mathrm{Re}\left[j\left(\boldsymbol{\psi}_{sdq+}^{+}\hat{\boldsymbol{I}}_{sdq3+}^{3+} + \boldsymbol{\psi}_{sdq-}^{-}\hat{\boldsymbol{I}}_{sdq+}^{+}\right)e^{-j2\theta_1}\right] \tag{12}$$

where ω_r is rotor electric angular speed, Ψ is flux, which can be presented as

$$\begin{aligned}\boldsymbol{\psi}_{sdq+}^{+} &= \frac{1}{\omega_1}\left(U_{sq+}^{+} - jU_{sd+}^{+}\right)\\ \boldsymbol{\psi}_{sdq-}^{-} &= \frac{1}{\omega_1}\left(-U_{sq-}^{-} + jU_{sd-}^{-}\right).\end{aligned} \tag{13}$$

Based on (8a) and (8b) and (13), (12) can be rewritten as

$$P_{e2}^I = \frac{3\omega_r}{\omega_1}\left(-A_1\cos 2\theta_1 - A_2\sin 2\theta_1\right) \tag{14a}$$

$$A_1 = U_{sd-}^{-}I_{sd+}^{+} + U_{sq-}^{-}I_{sq+}^{+};\quad A_2 = U_{sq-}^{-}I_{sd+}^{+} - U_{sd-}^{-}I_{sq+}^{+}. \tag{14b}$$

Similarly, the 300 Hz electromagnetic power pulsation can be presented as

$$P_{e6}^I = \frac{3}{2}\omega_r \mathrm{Re}\left[j\begin{pmatrix}\boldsymbol{\psi}_{sdq+}^{+}\hat{\boldsymbol{I}}_{sdq5-}^{5-}e^{j6\theta_1} + \boldsymbol{\psi}_{sdq7+}^{7+}\boldsymbol{I}_{sdq+}^{+}e^{j6\theta_1}\\ +\boldsymbol{\psi}_{sdq+}^{+}\hat{\boldsymbol{I}}_{sdq7+}^{7+}e^{-j6\theta_1} + \boldsymbol{\psi}_{sdq5-}^{5-}\hat{\boldsymbol{I}}_{sdq+}^{+}e^{-j6\theta_1}\end{pmatrix}\right]. \tag{15}$$

The fifth and seventh harmonic components of stator current under control Target I can be expressed as [10]

$$\begin{aligned}I_{sd5-}^{5-} &= \frac{-U_{sd7+}^{7+}I_{sd+}^{+} - U_{sq7+}^{7+}I_{sq+}^{+}}{U_{sd+}^{+}}\\ I_{sq5-}^{5-} &= \frac{U_{sq7+}^{7+}I_{sd+}^{+} - U_{sd7+}^{7+}I_{sq+}^{+}}{U_{sd+}^{+}}\\ I_{sd7+}^{7+} &= \frac{-U_{sd5-}^{5-}I_{sd+}^{+} - U_{sq5-}^{5-}I_{sq+}^{+}}{U_{sd+}^{+}}\\ I_{sq7+}^{7+} &= \frac{U_{sq5-}^{5-}I_{sd+}^{+} - U_{sd5-}^{5-}I_{sq+}^{+}}{U_{sd+}^{+}}.\end{aligned} \tag{16}$$

Then, (15) can be rewritten as

$$\begin{aligned}P_{e6}^I = {}& \frac{3}{2}\frac{\omega_r}{\omega_1}\left(\left(-\frac{6}{5}A_3 - \frac{6}{7}A_5\right)\cos 6\theta_1\right.\\ &\left.+\left(-\frac{6}{5}A_4 + \frac{6}{7}A_6\right)\sin 6\theta_1\right)\end{aligned} \tag{17a}$$

$$\begin{aligned}A_3 &= U_{sd5-}^{5-}I_{sd+}^{+} + U_{sq5-}^{5-}I_{sq+}^{+}\\ A_4 &= U_{sq5-}^{5-}I_{sd+}^{+} - U_{sd5-}^{5-}I_{sq+}^{+}\\ A_5 &= U_{sd7+}^{7+}I_{sd+}^{+} + U_{sq7+}^{7+}I_{sq+}^{+}\\ A_6 &= U_{sq7+}^{7+}I_{sd+}^{+} - U_{sd7+}^{7+}I_{sq+}^{+}.\end{aligned} \tag{17b}$$

As can be observed from (14a) and (14b) and (17a) and (17b), when the control Target I is achieved, the electromagnetic power would contain 100 and 300 Hz pulsation components P_{e2}^I and P_{e6}^I, while the DFIG stator power and GSC power P_s and P_g would both be smooth without pulsation, i.e., $P_{s2} = P_{s6} = P_{g2} = P_{g6} = 0$; thus, according to (11), the 100 and 300 Hz fluctuation of dc-link voltage under control Target I can be expressed as

$$C\frac{dV_{dc2}^I}{dt}V_{dc2}^I = P_{e2}^I;\quad C\frac{dV_{dc6}^I}{dt}V_{dc6}^I = P_{e6}^I. \tag{18}$$

2) Power Pulsation Under Control Target II: When control Target II is achieved, the balanced and sinusoidal stator and grid current would be ensured in the DFIG stator winding and GSC. Thus, the 100 Hz electromagnetic power pulsation can be presented as

$$\begin{aligned}P_{e2}^{II} &= \frac{3}{2}\omega_r \mathrm{Re}\left[j\left(\boldsymbol{\psi}_{sdq-}^{-}\boldsymbol{I}_{sdq+}^{+}\right)e^{-j2\theta_1}\right]\\ &= \frac{3\omega_r}{2\omega_1}\left(-A_1\cos 2\theta_1 - A_2\sin 2\theta_1\right)\end{aligned} \tag{19}$$

where A_1 and A_2 can be found in (14b).

According to [8], the DFIG stator active power and GSC active power would also contain the 100 Hz pulsation

$$P_{s2}^{II} = -\frac{3}{2}\left(A_1\cos 2\theta_1 + A_2\sin 2\theta_1\right) \tag{20}$$

$$P_{g2}^{II} = -\frac{3}{2}\begin{bmatrix}\left(U_{sd-}^{-}I_{gd+}^{+} + U_{sq-}^{-}I_{gq+}^{+}\right)\cos 2\theta_1\\ +\left(U_{sq-}^{-}I_{gd+}^{+} - U_{sd-}^{-}I_{gq+}^{+}\right)\sin 2\theta_1\end{bmatrix}. \tag{21}$$

Based on the 100 Hz electromagnetic power pulsation in (19), 100 Hz DFIG stator power pulsation in (20), 100 Hz GSC power pulsation in (21), it can be found out that

$$\begin{aligned}P_{e2}^{II} + P_{s2}^{II} + P_{g2}^{II} = {}& -\frac{3\left(\omega_r + \omega_1\right)}{2\omega_1}\left(A_1\cos 2\theta_1 + A_2\sin 2\theta_1\right)\\ &-\frac{3}{2}\left(\left(U_{sd-}^{-}I_{gd+}^{+} + U_{sq-}^{-}I_{gq+}^{+}\right)\cos 2\theta_1\right.\\ &\left.+\left(U_{sq-}^{-}I_{gd+}^{+} - U_{sd-}^{-}I_{gq+}^{+}\right)\sin 2\theta_1\right)\end{aligned} \tag{22}$$

The 300 Hz electromagnetic power pulsation under control Target II can be presented as

$$\begin{aligned} P_{e6}^{II} &= \frac{3}{2}\omega_r \mathrm{Re}\left(j\left(\boldsymbol{\psi}_{sdq5-}^{5-}e^{-j6\theta_1}+\boldsymbol{\psi}_{sdq7+}^{7+}e^{j6\theta_1}\right)\hat{\boldsymbol{I}}_{sdq+}^{+}\right) \\ &= \frac{3\omega_r}{2\omega_1}\Big(\frac{1}{7}A_5\cos 6\theta_1-\frac{1}{7}A_6\sin 6\theta_1-\frac{1}{5}A_3\cos 6\theta_1 \\ &\quad -\frac{1}{5}A_4\sin 6\theta_1\Big). \end{aligned} \tag{23}$$

The 300 Hz DFIG stator active power pulsation can be expressed as [10]

$$P_{s6}^{II}=-\frac{3}{2}\left(A_5\cos 6\theta_1-A_6\sin 6\theta_1+A_3\cos 6\theta_1+A_4\sin 6\theta_1\right). \tag{24}$$

Similarly, the 300 Hz GSC active power pulsation can be expressed as

$$P_{g6}^{II}=-\tfrac{3}{2}\begin{bmatrix}\left(U_{sd5-}^{5-}I_{gd+}^{+}+U_{sq5-}^{5-}I_{gq+}^{+}+U_{sd7+}^{7+}I_{gd+}^{+}\right.\\ \left.+U_{sq7+}^{7+}I_{gq+}^{+}\right)\cos 6\theta_1\\ +\left(U_{sq5-}^{5-}I_{gd+}^{+}-U_{sd5-}^{5-}I_{gq+}^{+}-U_{sq7+}^{7+}I_{gd+}^{+}\right.\\ \left.+U_{sd7+}^{7+}I_{gq+}^{+}\right)\sin 6\theta_1\end{bmatrix}. \tag{25}$$

Based on (23), (24), and (25), the 300 Hz power pulsation under control Target II can be expressed as

$$\begin{aligned} &P_{e6}^{II}+P_{s6}^{II}+P_{g6}^{II} \\ &=\frac{3}{2}\begin{bmatrix}\left(\frac{\omega_r}{7\omega_1}-1\right)A_5\cos 6\theta_1-\left(\frac{\omega_r}{7\omega_1}-1\right)A_6\sin 6\theta_1\\ -\left(\frac{\omega_r}{5\omega_1}+1\right)A_3\cos 6\theta_1-\left(\frac{\omega_r}{5\omega_1}+1\right)A_4\sin 6\theta_1\end{bmatrix} \\ &\quad -\frac{3}{2}\begin{bmatrix}(U_{sd5-}^{5-}I_{gd+}^{+}+U_{sq5-}^{5-}I_{gq+}^{+}+U_{sd7+}^{7+}I_{gd+}^{+}\\ +U_{sq7+}^{7+}I_{gq+}^{+})\cos 6\theta_1\\ +(U_{sq5-}^{5-}I_{gd+}^{+}-U_{sd5-}^{5-}I_{gq+}^{+}-U_{sq7+}^{7+}I_{gd+}^{+}\\ +U_{sd7+}^{7+}I_{gq+}^{+})\sin 6\theta_1\end{bmatrix}. \end{aligned} \tag{26}$$

Therefore, it can be found out that the power pulsation of 100 Hz under Target I in (14a) and (14b) and under Target II in (22) is different, while the power pulsation of 300 Hz under Target I in (17a) and (17b) and under Target II in (26) is also different.

However, it is reported in [1] that GSC provides the slip rate ($s=(\omega_1-\omega_r)/\omega_1$) percentage of DFIG output active power

$$\boldsymbol{I}_{gd+}^{+}=-s_l\boldsymbol{I}_{sd+}^{+} \tag{27}$$

where s_l is the slip rate, and the "$-$" indicates that the GSC power flows from grid to DFIG system under subsynchronous state ($s_l>0$), or from DFIG system to grid under supersynchronous state ($s_l<0$).

Then, under the special circumstance that both the RSC and GSC output zero reactive power, i.e., $I_{sq+}^{+}=0$, $I_{gq+}^{+}=0$, and according to (27), the active power pulsation of 100 Hz under Target II in (22) can be transformed into the same as the active power pulsation of 100 Hz under Target I in (14a) and (14b). Similarly, the active power pulsation of 300 Hz under Target II in (26) can also be transformed into the same as the active power pulsation of 300 Hz under Target I in (17a) and (17b).

3) DC-Link Voltage Fluctuation Analysis: Undoubtedly, the active power pulsation of 100 and 300 Hz under Targets I and II would both result in the dc-link voltage fluctuation, and for the sake of discussion simplicity, only the case of special circumstance (i.e., $I_{sq+}^{+}=0$, $I_{gq+}^{+}=0$) would be analyzed here, where both the 100 and 300 Hz power pulsation under control Targets I and II are the same; thus, the corresponding 100 and 300 Hz dc-link voltage fluctuation would be the same no matter which control target is selected under this special circumstance.

The dc-link voltage can be expressed including the dc component, 100 and 300 Hz fluctuation components as follows:

$$\begin{aligned} V_{dc} &= V_{dc0}+V_{dc2\cos}\cos 2\theta_1+V_{dc2\sin}\sin 2\theta_1 \\ &\quad +V_{dc6\cos}\cos 6\theta_1+V_{dc6\sin}\sin 6\theta_1 \\ &= V_{dc0}+V_{dc2m}\sin(2\theta_1+\varphi_2)+V_{dc6m}\sin(6\theta_1+\varphi_6) \end{aligned} \tag{28a}$$

where V_{dc0} represents the dc component, V_{dc2cos}, V_{dc2sin} represents the 100 Hz cosine and sine fluctuation component, V_{dc6cos}, V_{dc6sin} represents the 300 Hz cosine and sine fluctuation component, V_{dc2m}, V_{dc6m} represents the overall 100 and 300 Hz fluctuation component, which can be calculated according to the trigonometric function as

$$\begin{aligned} V_{dc2m} &= \sqrt{(V_{dc2\cos})^2+(V_{dc2\sin})^2} \\ V_{dc6m} &= \sqrt{(V_{dc6\cos})^2+(V_{dc6\sin})^2}. \end{aligned} \tag{28b}$$

Based on (28a) and (28b), the dc-link voltage fluctuation in (11) can be rewritten as

$$\begin{aligned} C\frac{dV_{dc}}{dt}V_{dc} &= C\big(2\omega_1 V_{dc2m}\cos(2\theta_1+\varphi_2) \\ &\quad +6\omega_1 V_{dc6m}\cos(6\theta_1+\varphi_6)\big) \\ &\quad *\big(V_{dc0}+V_{dc2m}\sin(2\theta_1+\varphi_2) \\ &\quad +V_{dc6m}\sin(6\theta_1+\varphi_6)\big). \end{aligned} \tag{29}$$

According to the 100 Hz power pulsation under control Targets I and II as given in (14a) and (14b) and (22), the 100 Hz dc-link voltage fluctuation in (29) can be presented as

$$\begin{aligned} &2\omega_1 C V_{dc0}V_{dc2m}\sin(2\theta_1+\varphi_2) \\ &=\frac{3\omega_r}{\omega_1}\sqrt{A_1^2+A_2^2}\sin(2\theta_1+\varphi_3). \end{aligned} \tag{30}$$

Thus, the 100 Hz dc-link voltage fluctuation can be obtained as

$$V_{dc2m}=\frac{3\omega_r\sqrt{A_1^2+A_2^2}}{2(\omega_1)^2 C V_{dc0}}. \tag{31a}$$

The 300 Hz dc-link voltage fluctuation can be deduced similarly on the basis of (17a) and (17b) and (26) and shown as

$$V_{dc6m} = \frac{\omega_r \sqrt{(-(6/5)A_3 - (6/7)A_5)^2 + (-(6/5)A_4 + (6/7)A_6)^2}}{4(\omega_1)^2 C V_{dc0}}. \tag{31b}$$

Finally, (31a) and (31b) give out the 100 and 300 Hz dc-link voltage fluctuation under the special circumstance using the modularized control strategy. It can be concluded from (31a) and (31b) that:

1) DC-link voltage fluctuation would become more severe when the rotor speed ω_r accelerates from subsynchronous state to the supersynchronous state.
2) DC component $V_{\rm dc0}$ in dc-link voltage would also influence the 100 and 300 Hz fluctuation component, and larger $V_{\rm dc0}$ would be helpful in reducing the voltage fluctuation.
3) The 100 Hz fluctuation caused by grid voltage unbalance would be comparatively larger than the 300 Hz fluctuation; therefore, the grid voltage unbalance rather than the harmonic distortion should deserve more attention in the practical situation.
4) When the grid voltage negative component $\boldsymbol{U}^{-}_{sdq-}$, harmonic components $\boldsymbol{U}^{5-}_{sdq5-}$ and $\boldsymbol{U}^{7+}_{sdq7+}$, and the stator current fundamental component $\boldsymbol{I}^{+}_{sdq+}$ increase, the corresponding dc-link voltage fluctuation would also increase.
5) According to (31a) and (31b), a proper dc-link capacitor can be designed to satisfy the dc-link voltage fluctuation criterion for the reliable operation of DFIG system under the nonideal grid voltage condition.

C. Electromagnetic Torque Pulsation Under Target I and Target II

When DFIG operates under the unbalanced and harmonic voltage, the smooth electromagnetic torque is usually set as the important control target for the reliable working of the mechanic parts, i.e., the gear-box and DFIG rotor shaft and bearing. Since the balanced and sinusoidal current, or smooth output power, is achieved for DFIG in this paper, 100 and 300 Hz fluctuation of electromagnetic torque will occur inevitably.

As deduced in Section IV-B, the 100 and 300 Hz fluctuation of electromagnetic power under control Targets I and II has been given in (14a) and (14b), (17a) and (17b), (19), and (23). And the electromagnetic torque can be presented as

$$T_e = \frac{P_e}{p\omega_r} \tag{32}$$

where T_e is electromagnetic torque and p is the DFIG pole pairs.

Therefore, based on (14a) and (14b), (17a) and (17b), and (32), 100 and 300 Hz pulsation of the electromagnetic torque under control Target I can be expressed as

$$T^I_{e2} = \frac{3}{p\omega_1}\left(-A_1\cos 2\theta_1 - A_2 \sin 2\theta_1\right) \tag{33a}$$

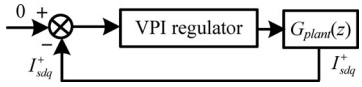

Fig. 2. Closed-loop control scheme using VPI regulator with control Target II.

$$T^I_{e6} = \frac{3}{2p\omega_1}\left(\left(-\frac{6}{5}A_3 - \frac{6}{7}A_5\right)\cos 6\theta_1 + \left(-\frac{6}{5}A_4 + \frac{6}{7}A_6\right)\sin 6\theta_1\right). \tag{33b}$$

Similarly, based on (19), (23), and (32), 100 and 300 Hz pulsation of the electromagnetic torque under control Target II can be expressed as

$$T^{II}_{e2} = \frac{3}{2p\omega_1}\left(-A_1\cos 2\theta_1 - A_2 \sin 2\theta_1\right) \tag{34a}$$

$$T^{II}_{e6} = \frac{3}{2p\omega_1}\left(\left(-\frac{1}{5}A_3 + \frac{1}{7}A_5\right)\cos 6\theta_1 + \left(-\frac{1}{5}A_4 - \frac{1}{7}A_6\right)\sin 6\theta_1\right). \tag{34b}$$

According to the electromagnetic torque pulsation expression shown in (33) and (34), the following conclusion can be obtained:

1) Based on A_1–A_6 shown in (14b) and (17b), as the grid voltage unbalance and distortion become severe, the larger electromagnetic torque pulsation will occur.
2) It can be found out that the 100 Hz electromagnetic torque pulsation under control Target II is half as that under control Target I. Moreover, the 300 Hz electromagnetic torque pulsation under control Target II is also much smaller than that under control Target I; therefore, it can be verified that the overall electromagnetic torque pulsation under control Target II would be much smaller than that under control Target I.

D. VPI Regulator's Robustness Against DFIG Parameter Deviation

In the practical application, the DFIG parameter deviation may occur due to the temperature changing, skin effect or flux saturation, thus discussing the VPI regulator's robustness against DFIG parameter deviation would be essential, and for the sake of simplicity, the control Target II of balanced and sinusoidal stator current is taken as an example.

When the control Target II of balanced and sinusoidal stator current is implemented, the closed-loop control scheme can be shown in Fig. 2.

The transfer function of control subject DFIG from VPI regulator output to stator current can be presented as

$$G_{plant}(s) = \frac{L_m}{L_s}\frac{1}{R_r + s\sigma L_r} \tag{35}$$

where R_r is DFIG rotor resistance, $\sigma = 1–L2m/L_sL_r$ is DFIG leakage inductance efficient, and L_r is the DFIG rotor inductance.

Then, the closed-loop control transfer function can be presented as (36), shown at the bottom of the page.

Preliminarily, it should be noted that the leakage inductance efficient σ is calculated as

$$\sigma = 1 - \frac{L_m^2}{L_s L_r} \tag{37}$$

where L_s is the stator inductance, L_r is the rotor inductance, and L_m is the mutual inductance.

The stator inductance and rotor inductance can be, respectively, presented as

$$L_s = L_m + L_{\sigma s}; \qquad L_r = L_m + L_{\sigma r} \tag{38}$$

where $L_{\sigma s}$ is the stator leakage inductance and $L_{\sigma r}$ is the rotor leakage inductance; $L_{\sigma s}$ and $L_{\sigma r}$ are almost equal.

Thus, based on the transfer function of control subject DFIG, the rotor resistance R_r, mutual inductance L_m, and leakage inductance L_σ (designating both $L_{\sigma s}$ and $L_{\sigma r}$) would be involved in the discussion of VPI regulator's robustness against DFIG parameter deviation. Typically, the variation range of mutual inductance L_m, leakage inductance L_σ, and rotor resistance R_r is chosen, respectively, as $\pm 20\%$, $\pm 60\%$, and $\pm 50\%$ [21]. The corresponding bode diagram of closed-loop control transfer function with the different parameter deviation is shown in Fig. 3.

As can be observed from Fig. 3(a), once the mutual inductance L_m deviates to 0.8 times or 1.2 times of the normal value, both the closed-loop magnitude response and phase response within 50–350 Hz would remain almost unchanged, and more importantly, the magnitude response at 100 and 300 Hz would maintain 0 dB, and the phase response at 100 and 300 Hz would remain 0°. As shown in Fig. 3(b), when the leakage inductance L_σ deviation of $\pm 60\%$ occurs, the slight changing of magnitude response and phase response within 50–350 Hz can be observed, while the magnitude and phase response at the control frequency of 100 and 300 Hz would remain 0 dB and 0°. When the rotor resistance R_r deviation of $\pm 50\%$ happens, as given in Fig. 3(c), the magnitude and phase response can keep almost same, and the magnitude and phase response of 0 dB and 0° at the control frequency 100 and 300 Hz can be ensured. Therefore, based on the analysis result shown in Fig. 3, it can be found out that the effective working capability of VPI regulator under the circumstance of DFIG parameters deviation can be guaranteed, and the achievement of the control targets can be obtained.

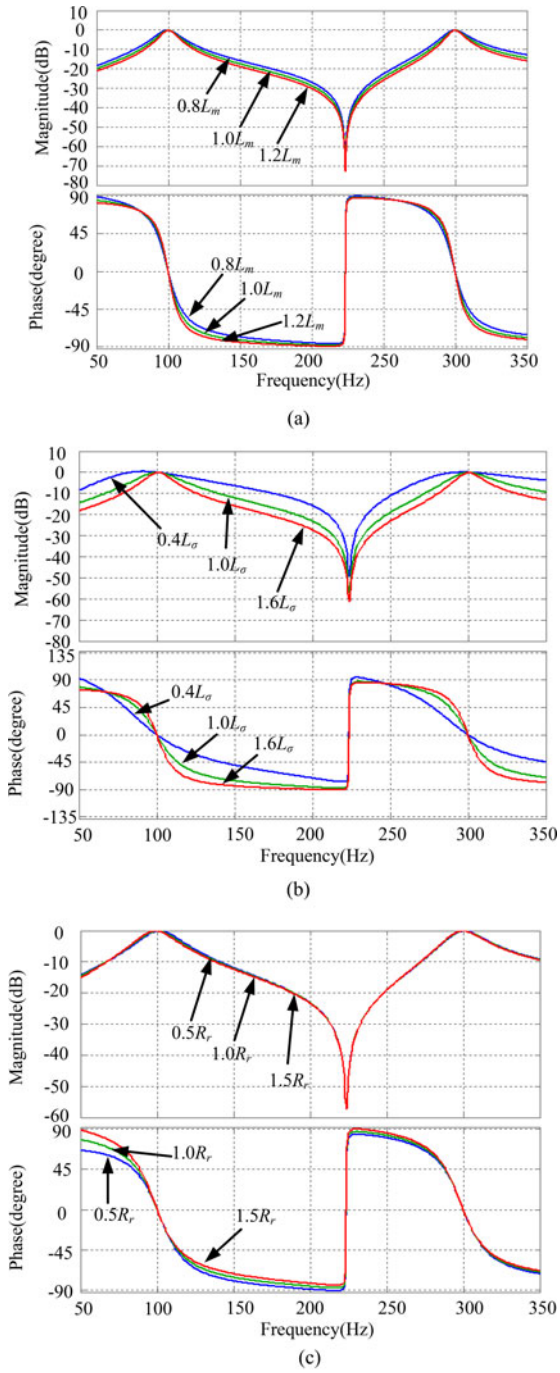

Fig. 3. Bode diagram of closed-loop control transfer function with DFIG parameter deviation (a) mutual inductance L_m deviation of $\pm 20\%$; (b) leakage inductance L_σ deviation of $\pm 60\%$; (b) rotor resistance R_r deviation of $\pm 50\%$ (VPI regulator parameters of $\omega_{c6} = \omega_{c6} = 2$ rad/s, $K_{pr2} = K_{pr6} = 1$, $K_{ir2} = K_{ir6} = 150$).

$$C_{cl}(s) = \frac{C_{VPI}(s)G_{plant}(s)}{1 + C_{VPI}(s)G_{plant}(s)} = \frac{\left((K_{pr2}s^2 + K_{ir2}s)/(s^2 + \omega_{c2}s + (2\omega_1)^2) + (K_{pr6}s^2 + K_{ir6}s)/(s^2 + \omega_{c6}s + (6\omega_1)^2)\right)(L_m/L_s)(1/(R_r + s\sigma L_r))}{1 + \left((K_{pr2}s^2 + K_{ir2}s)/(s^2 + \omega_{c2}s + (2\omega_1)^2) + (K_{pr6}s^2 + K_{ir6}s)/(s^2 + \omega_{c6}s + (6\omega_1)^2)\right)(L_m/L_s)(1/(R_r + s\sigma L_r))} \tag{36}$$

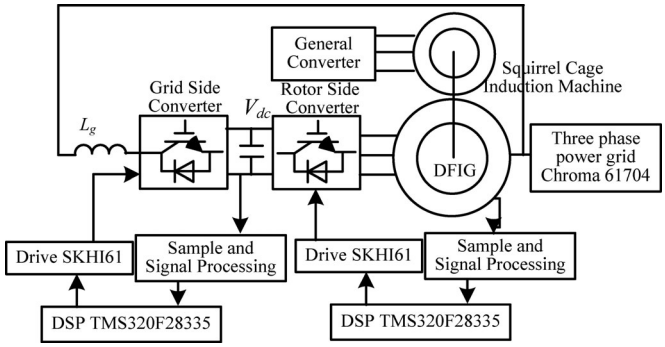

Fig. 4. Block diagram of experiment system.

TABLE I
PARAMETERS OF EXPERIMENT DFIG SYSTEM

Rated Power	1 kW	Frequency	50 Hz
Grid voltage	110 V	DFIG pole pairs	3
Stator/rotor turns ratio	0.33	DC-link voltage V_{dc}	200 V
Stator resistance R_s	1.01 Ω	DC-link capacitor C_{dc}	2200 μF
Rotor resistance R_r	0.88 Ω	GSC line inductance L_g	4 mH
DFIG mutual inductance L_m	90.1 mH	GSC line resistance R_g	0.02 Ω
DFIG stator leakage inductance $L_{\sigma s}$	3.0 mH	DFIG rotor leakage inductance $L_{\sigma r}$	3.0 mH

V. EXPERIMENTAL VALIDATION

A. Experiment Setup

Experiment system was built on a laboratory prototype of 1 kW DFIG system as shown in Fig. 4, the DFIG is driven by a 1.5 kW squirrel cage induction machine as the wind turbine. The induction machine is driven by a general converter. The Chroma 61704 is employed to simulate the practical unbalanced and harmonically distorted power grid. In the experiment, grid voltage negative, fifth, and seventh-order harmonic components are set 2.90%, 2.36%, and 1.17%, respectively. The parameters of the DFIG system are listed in Table I.

In the control of DFIG RSC, the rotor speed is initially set to 800 r/min (the synchronous speed is 1000 r/min). The dc-link voltage is provided by the GSC to be 200 V. Both the RSC and GSC control strategies are implemented on the two separate DSP TMS320F28335, and the driver for IGBT is SEMIKRON SKHI61. The sampling frequency is 10 kHz, and the IGBT switching frequency is 5 kHz.

B. Experiment Results

Fig. 5 shows the experimental result of DFIG system under unbalanced and distorted grid voltage condition when VPI regulator is disabled. It can be found out that the heavily unbalanced and distorted current in GSC and DFIG will occur; moreover, 100 and 300 Hz pulsation of the GSC and DFIG stator power would be produced; the detailed experiment result analysis can be found in Table II.

Fig. 6 shows the experimental result of DFIG system under unbalanced and distorted grid voltage condition with control

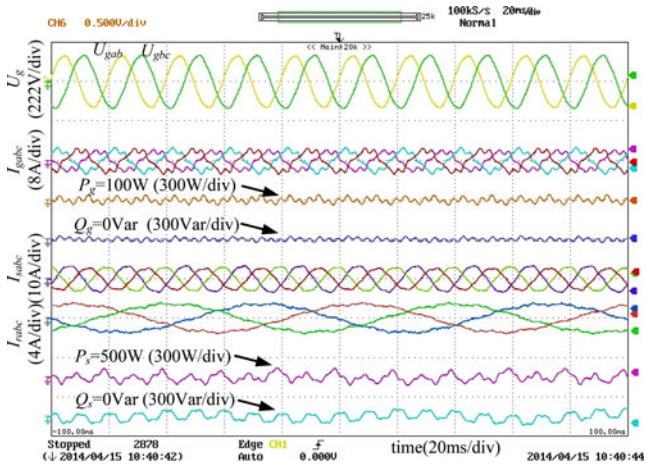

Fig. 5. Experimental result of DFIG system performance under unbalanced and distorted grid voltage condition when VPI regulator is disabled.

TABLE II
EXPERIMENT RESULT ANALYSIS

	Without VPI Control	Control Target I	Control Target II
U_g negative	2.90%	2.90%	2.90%
U_g fifth order	2.36%	2.36%	2.36%
U_g seventh order	1.17%	1.17%	1.17%
I_g negative	13.82%	1.22%	1.62%
I_g third order	1.62%	4.70%	1.18%
I_g fifth order	14.49%	6.02%	2.31%
I_g seventh order	13.39%	2.88%	1.84%
P_g 100 Hz	±84 W	±10 W	±27 W
Q_g 100 Hz	±18 Var	±9 Var	±15 Var
P_g 300 Hz	±36 W	±5 W	±30 W
Q_g 300 Hz	±30 Var	±4 Var	±24 Var
I_s negative	17.42%	1.56%	1.69%
I_s third order	0.45%	5.41%	0.31%
I_s fifth order	4.37%	2.79%	1.85%
I_s seventh order	1.87%	2.01%	0.92%
P_s 100 Hz	±84 W	±18 W	±45 W
Q_s 100 Hz	±75 Var	±25 Var	±45 Var
P_s 300 Hz	±36 W	±12 W	±30 W
Q_s 300 Hz	±24 Var	±10 Var	±21 Var

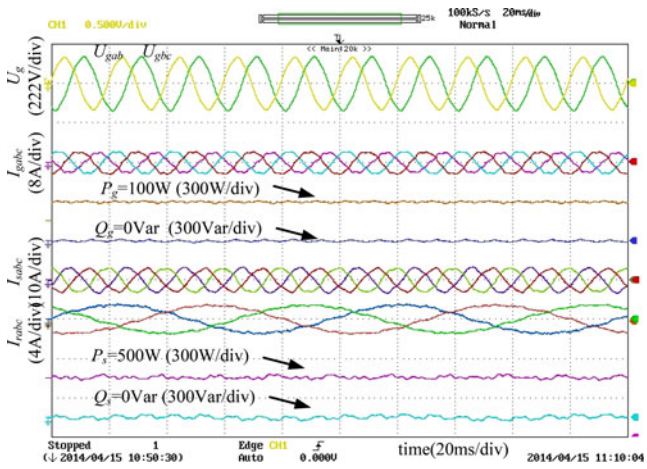

Fig. 6. Experimental result of DFIG system under unbalanced and distorted grid voltage condition with control Target I.

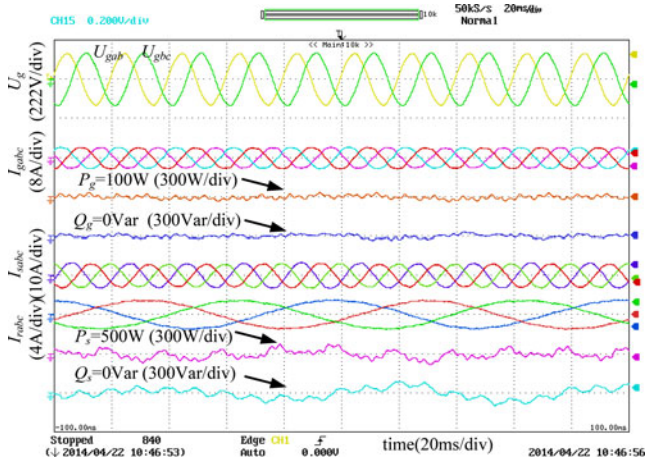

Fig. 7. Experimental result of DFIG system under unbalanced and distorted grid voltage condition with control Target II.

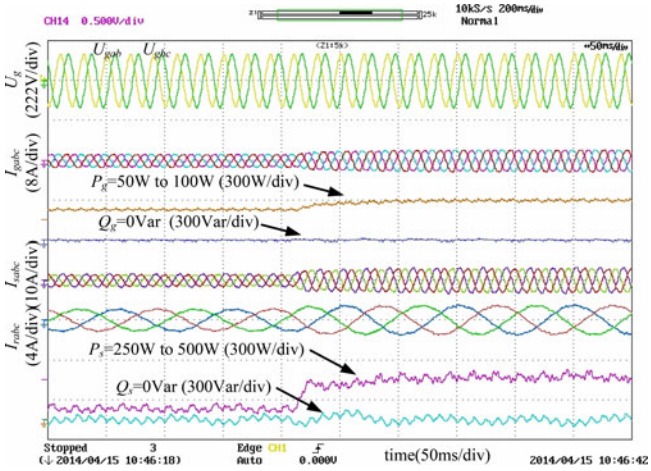

Fig. 8. Experimental result of DFIG stator output active power stepping under unbalanced and distorted grid voltage condition with control Target II: balanced and sinusoidal GSC three-phase current and DFIG stator current.

Target I, i.e., the smooth GSC output power and smooth DFIG stator output power is achieved. As can be seen, the GSC power and DFIG stator power would all become much smoother compared with the results in Figs. 5 and 7. It can also be seen from Table II that, in order to eliminate the 100 Hz GSC power and DFIG stator power pulsation, both the GSC current and DFIG stator current would contain nonnegligible amount of the third harmonic component. Similarly, for the purpose of removing the 300 Hz power pulsation, the GSC current and DFIG stator current would contain the severe fifth and seventh harmonic components compared with the result shown in Fig. 7. The detailed experiment result analysis is also available in Table II.

Fig. 7 shows the experimental result of DFIG system under unbalanced and distorted grid voltage condition with control Target II, i.e., the balanced and sinusoidal GSC current and DFIG stator current is achieved. In comparison with Fig. 5, both the GSC three-phase current and DFIG stator current would be significantly improved with negligible harmonic distortion and tiny unbalance; this is quite helpful for the safe and reliable operation of the power grid. Besides, the pulsation of GSC power and DFIG stator output power would also be larger than that under control Target I. The detailed experiment result analysis is available in Table II.

By analyzing the experiment results, it can be found out in Table II that compared with the control without VPI regulator, the unbalanced and distorted current, as well as power pulsation can be significantly improved whatever control target is implemented. Moreover, the pulsation of DFIG stator output active/reactive power and GSC active/reactive power under control Target I is much smaller than that under control Target II. Instead, the heavily distorted DFIG stator current and GSC current, containing third, fifth, and seventh harmonic components, would be generated under Target I as a consequence. It should be noted that no negative component of DFIG stator current or GSC current would occur under both control targets, which verifies the theoretical analysis in Section IV-A.

Fig. 8 shows the experimental result of DFIG stator output active power stepping from 250 to 500 W with control Target II, and the GSC active power would correspondingly step from 50 to 100 W. It can be seen that the DFIG stator active power stepping takes the transient response time of around 100 ms, which proves the excellent dynamic regulation capability of the rotor current fundamental component. Moreover, it can be observed that the GSC current and DFIG stator current is able to maintain balanced and sinusoidal both before and after the stepping moment; this result validates the proposed modularized control strategy by applying the VPI closed-loop control.

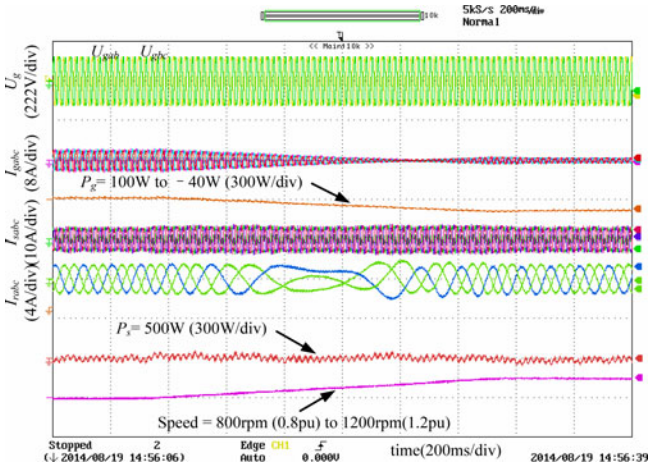

Fig. 9. Experimental result of DFIG speeding up from 800 r/min (0.8 p.u.) to 1200 r/min (1.2 p.u.) under unbalanced and distorted grid voltage condition with control Target II: balanced and sinusoidal GSC three-phase current and DFIG stator current.

Fig. 9 shows the experimental result of DFIG speeding up from 800 r/min (0.8 p.u.) to 1200 r/min (1.2 p.u.) under unbalanced and distorted grid voltage condition with control Target II: balanced and sinusoidal GSC three-phase current and DFIG stator current. As can be seen from Fig. 9, when the rotor speed acceleration happened, the GSC current would first decrease to 0, then the direction of GSC current would become opposite, indicating that the GSC would operate as an inverter under

supersynchronous state, and the GSC power would flow from the dc-link capacitor to the power grid. Importantly, it should be noted that since the several losses (copper loss, magnetizing loss) in the experiment inevitably exists; therefore, the magnitude of GSC current under subsynchronous state would be smaller than that under supersynchronous state ($P_g = 100$ to -40 W) due to these losses. Moreover, the stator current is able to maintain constant within the DFIG speeding moment, and the stator output power can also remain constant as a result. The rotor current, which is relevant to the DFIG rotor speed, would change according to the speeding variation with very smooth transient response, and no overcurrent or overshoot can be observed. Thus, it can be concluded that the proposed control strategy is able to maintain effective under the circumstance of DFIG speed variation, thus making the strategy applicable in the practical situation where DFIG speed variation happens frequently.

VI. Conclusion

The paper presented a modularized control strategy of the DFIG system under unbalanced and distorted grid voltage, with the control targets of smooth active and reactive power of RSC and GSC, or balanced and sinusoidal current for both RSC and GSC. Several advantages over the conventional control strategy have been validated: 1) avoids the negative and harmonic component extraction in GSC and RSC; 2) removes the complicated and time-consuming current reference calculation; and 3) is able to cancel the communication between RSC and GSC. It has been proved that when the smooth active and reactive power is achieved, no negative component of current would be generated, but only third harmonic current component occurs, which would unfortunately further pollute the power grid. However, the 100 and 300 Hz dc-link voltage fluctuation would be generated when control Targets I and II are achieved; the electromagnetic torque 100 and 300 Hz pulsation under control Targets I and II have also been theoretically analyzed. Besides, it has also been proved that the VPI regulator has strong robustness against DFIG parameters deviation.

References

[1] S. Muller, M. Deicke, and R. W. De Doncker, "Doubly fed induction generator systems for wind turbines," *IEEE Ind. Appl. Mag.*, vol. 8, no. 3, pp. 26–33, May/Jun. 2002.

[2] D. Zhi and L. Xu, "Direct power control of DFIG with constant switching frequency and improved transient performance," *IEEE Trans. Energy Convers.*, vol. 22, no. 2, pp. 110–118, Mar. 2007.

[3] National Grid Transco, Appendix 1. (Feb. 2004). *Extracts from the grid code—Connection conditions* [Online]. Available: http://www.nationalgrid.com

[4] *IEEE Recommended Practices and Requirements for Harmonic Control in Electrical Power Systems*, IEEE Standard 519-1992, 1993.

[5] J. Hu, H. Xu, and Y. He, "Coordinated control of DFIG's RSC and GSC under generalized unbalanced and distorted grid voltage conditions," *IEEE Trans. Ind. Electron.*, vol. 60, no. 7, pp. 2808–2819, Jul. 2013.

[6] H. Xu, J. Hu, and Y. He, "Integrated modeling and enhanced control of DFIG under unbalanced and distorted grid voltage conditions," *IEEE Trans. Energy Convers.*, vol. 27, no. 3, pp. 725–736, Sep. 2012.

[7] C. Liu, D. Xu, N. Zhu, F. Blaabjerg, and M. Chen, "DC-voltage fluctuation elimination through a DC-capacitor current control for DFIG converters under unbalanced grid voltage conditions," *IEEE Trans. Power Electron.*, vol. 28, no. 7, pp. 3206–3218, Jul. 2013.

[8] J. Hu, Y. He, L. Xu, and B. W. Williams, "Improved control of DFIG systems during network unbalance using PI–R current regulators," *IEEE Trans. Ind. Electron.*, vol. 56, no. 2, pp. 439–451, Feb. 2009.

[9] J. Yao, H. Li, Z. Chen, X. Xia, X. Chen, Q. Li, and Y. Liao, "Enhanced control of a DFIG-based wind-power generation system with series grid-side converter under unbalanced grid voltage conditions," *IEEE Trans. Power Electron.*, vol. 28, no. 7, pp. 3167–3181, Jul. 2013.

[10] J. Hu, H. Nian, H. Xu, and Y. He, "Dynamic modeling and improved control of DFIG under distorted grid voltage conditions," *IEEE Trans. Energy Convers.*, vol. 26, no. 1, pp. 163–175, Mar. 2011.

[11] H. Xu, J. Hu, and Y. He, "Operation of wind-turbine-driven DFIG systems under distorted grid voltage conditions: Analysis and experimental validations," *IEEE Trans. Power Electron.*, vol. 27, no. 5, pp. 2354–2366, May 2012.

[12] P. Zhou, Y. He, and D. Sun, "Improved direct power control of a DFIG-based wind turbine during network unbalance," *IEEE Trans. Power Electron.*, vol. 24, no. 11, pp. 2465–2474, Nov. 2009.

[13] H. Nian, Y. Song, P. Zhou, and Y. He, "Improved direct power control of a wind turbine driven doubly fed induction generator during transient grid voltage unbalance," *IEEE Trans. Energy Convers.*, vol. 26, no. 3, pp. 976–986, Sep. 2011.

[14] H. Nian and Y. Song, "Direct power control of doubly fed induction generator under distorted grid voltage," *IEEE Trans. Power Electron.*, vol. 29, no. 2, pp. 894–905, Feb. 2014.

[15] J. Hu, J. Zhu, Y. Zhang, G. Platt, Q. Ma, and D. G. Dorrell, "Predictive direct virtual torque and power control of doubly fed induction generators for fast and smooth grid synchronization and flexible power regulation," *IEEE Trans. Power Electron.*, vol. 28, no. 7, pp. 3182–3194, Jul. 2013.

[16] Y. Zhang, J. Hu, and J. Zhu. "Three-vectors-based predictive direct power control of the doubly fed induction generator for wind energy applications," *IEEE Trans. Power Electron.*, vol. 29, no. 7, pp. 3485–3500, Jul. 2014.

[17] C. Liu, F. Blaabjerg, W. Chen, and D. Xu, "Stator current harmonic control with resonant controller for doubly fed induction generator," *IEEE Trans. Power Electron.*, vol. 27, no. 7, pp. 3207–3220, Jul. 2012.

[18] Y. Song and H. Nian, "Comparison of resonant current regulators for DFIG during grid voltage distortion," *J. Zhejiang Univ-Sci C (Comput & Electron)*, vol. 14, no. 12, pp. 953–965, Dec. 2013.

[19] C. Lascu, L. Asiminoaei, I. Boldea, and F. Blaabjerg, "High performance current controller for selective harmonic compensation in active power filters," *IEEE Trans. Power Electron.*, vol. 22, no. 5, pp. 1826–1835, Sep. 2007.

[20] C. Lascu, L. Asiminoaei, I. Boldea, and F. Blaabjerg, "Frequency response analysis of current controllers for selective harmonic compensation in active power filters," *IEEE Trans. Ind. Electron.*, vol. 56, no. 2, pp. 337–347, Feb. 2009.

[21] H. M. Jabr and N. C. Kar. "Effects of main and leakage flux saturation on the transient performances of doubly-fed wind driven induction generator," *Electric Power Syst. Res.*, vol. 77, no. 8, pp 1019–1027, Jun. 2007.

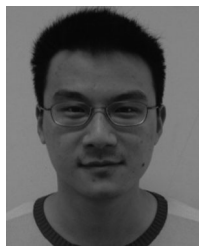

Yipeng Song (S'14) was born in Hangzhou, China. He received the B.Sc. degree in July 2010 from the College of Electrical Engineering, Zhejiang University, Hangzhou, China, where he is currently working toward the Ph.D. degree.

His current research interests include motor control with power electronics devices in renewable-energy conversion, particularly the control and operation of doubly fed induction generators for wind power generation under adverse grid condition.

Heng Nian (M'09) received the B.Eng. degree and the M.Eng. degree from Hefei University of Technology, Hefei, China, in 1999 and 2002, respectively, and the Ph.D. degree from Zhejiang University, Hangzhou, China, in 2005, all in electrical engineering.

From 2005 to 2007, he was as a Postdoctoral Fellow with the College of Electrical Engineering, Zhejiang University, China, where he has been an Associate Professor at the College of Electrical Engineering since 2007. His current research interests include the optimal design and operation control for wind power generation system.